Vibrational Relaxation of OH and OD Stretching Vibrations of Phenol and Its Clusters Studied by IR−UV Pump−Probe Spectroscopy

Takayuki Ebata,* Atsushi Iwasaki, and Naohiko Mikami

Department of Chemistry, Graduate School of Science, Tohoku University, Sendai 980-8578, Japan

Received: April 19, 2000; In Final Form: June 26, 2000

The vibrational relaxation of the OH/OD stretching mode of phenol and its cluster with Ar or H_2O has been observed directly by nanosecond IR−UV pump−probe spectroscopy. The OH/OD vibrational level was prepared by a tunable nanosecond IR light pulse, and the decay of the pumped level as well as the rise of the relaxed level were observed by two-photon ionization with a tunable UV laser. For the OH stretch level of phenol-d_0, two components were observed: a fast component with a decay time of a few nanoseconds and a slow component with a decay time longer than 1 μs. It was also found that the decay rate of the fast component coincides with that of the rise of relaxed levels. The results indicate that the intramolecular vibrational redistribution (IVR) of the OH stretching vibration of bare phenol-d_0 is classified as an intermediate-strong-coupling case. For phenol-d_1, only the slow component was identified for the decay of the OD stretching vibration, whereas the relaxed level showed a rise with a few nanoseconds, similar to the case of phenol-d_0. In the case of phenol−Ar and phenol−H_2O, on the other hand, the OH stretching level showed a fast single-exponential decay curve, indicating a transformation from intermediate coupling to the statistical limit upon the cluster formation.

Introduction

The OH stretching vibration of organic acids is known to be a peculiar mode from the perspective that it is almost isolated from other vibrational modes of the molecule, whereas it couples substantially with the intermolecular modes upon hydrogen-bond formation in the condensed phase. In vibrational spectra in the condensed phase, the OH stretching vibration often exhibits a large shift to lower frequency as well as a substantial broadening of its bandwidth,[1] which is in sharp contrast to the behavior of other modes such as CH stretching vibrations. The shift is essentially understood as the weakening of the OH bond induced by hydrogen-bond formation. For the spectral broadening, on the other hand, many factors are involved: a heterogeneous broadening due to spectral congestion because of the different circumstances of each OH group in the phase and a homogeneous broadening involving dynamics of the vibration such as dephasing and/or population decay. Although the origin of the broadening has been extensively studied experimentally and theoretically,[2−7] it is sometimes very difficult to provide an unambiguous interpretation in the bulk system because of the lack of microscopic structural information. In this respect, measurements of the broadening and the decay of the OH stretching vibration of the bare molecule and its hydrogen-bonded clusters, whose structures have been already well-characterized, may provide us with a fundamental model for the investigation of the dynamics of OH stretching vibrations occurring in condensed phases.

Very recently, we reported IR spectra of the OH stretching vibration of hydrogen-bonded clusters of phenol,[8−11] 2-naphthol,[12,13] tropolone,[14] methyl salicilate,[15] and benzyl alcohol[16,17] with various solvent molecules, such as water, methanol, ammonia, etc. The spectra of the OH stretching vibrations not only of the solute but also of the solvent molecules were observed for the size-specified clusters. Then, their geometrical structures and hydrogen-bonding network structures were unambiguously determined by comparison of the observed vibrational spectra with the simulated spectra obtained through ab initio molecular orbital calculations.

The vibrational relaxation of the OH stretching vibration of phenol and its clusters in S_0 has been investigated by Felker's group[18] and by Fujii's group.[19] The former group observed the OH stretch vibration of bare phenol and phenol−H_2O by ionization-detected stimulated Raman spectroscopy (IDSRS) and estimated the lifetimes from the bandwidths of the OH Raman band. The latter group observed the vibrational relaxation of bare phenol by using IR−UV double-resonant spectroscopy with nonresonant ionization detection (IR-NID). However, up to now, no direct observation of the time profile of the vibrational level has been reported.

In the present work, we report the direct observation of the decay profiles of the OH stretching vibration of phenol and its clusters in S_0. Time-resolved IR-pump and UV-probe spectroscopy was employed for observing the vibrational relaxation of the OH/OD stretch level of bare phenol-d_0 (phenol-d_1) and its clusters. A tunable nanosecond IR light pulse pumped the phenol molecules to their OH/OD stretch level, and the decay profile of the pumped level was directly observed by probing the transitions from the level by means of multiphoton ionization (MPI) with a UV light pulse. We also observed the rise of the electronic transition of the relaxed levels. We report the rate at which intramolecular vibrational redistribution (IVR) occurs after the IR excitation to the OH (OD) stretch level for bare phenol (phenol-d_1). We then examine how IVR is accelerated upon the cluster formation in the cases of phenol−Ar and phenol−H_2O, as examples. In the former cluster, although the interaction between the OH stretching and the van der Waals (vdW) modes is very weak, the vdW modes act as effective bath modes for accelerating the rate of IVR. In the latter cluster, the interaction between the OH stretch and the intermolecular modes is very strong, so that much faster IVR takes place. We

10.1021/jp0015022 CCC: $19.00
Published on Web 08/04/2000

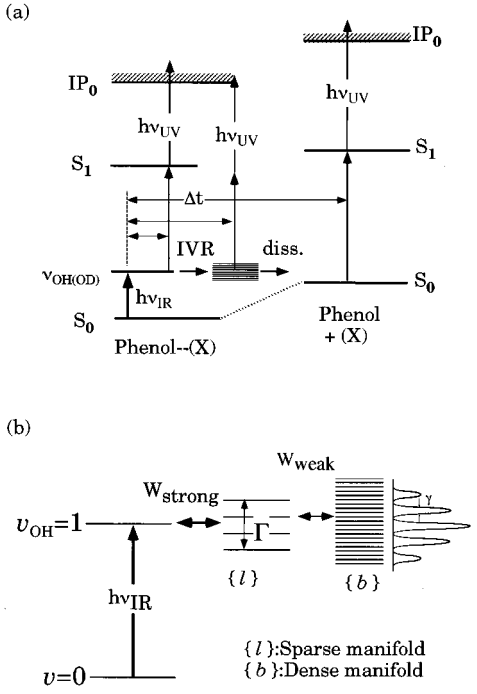

Figure 1. (a) Energy levels of phenol and its cluster and an excitation schemes of IR−UV pump−probe spectroscopy. (b) Coupling scheme among the OH stretching vibration, the sparse manifold, and the dense manifold.

discuss the effect of cluster formation on the decay of the OH stretching level.

Experimental Section

The setup for the IR−UV pump and probe experiment is essentially the same as those reported for the IR − UV double-resonant spectroscopy,[8−17] except that we observed transitions starting from the vibrationally excited level. Figure 1 shows the excitation scheme of the spectroscopy and the coupling scheme between the optically pumped OH/OD stretching vibration and the bath modes. A tunable IR pulse first pumps jet-cooled molecules to the OH/OD stretch level, and at a certain delay time, the UV light pulse is introduced to probe the OH/OD stretch level by 1 + 1 resonant-enhanced MPI (REMPI) via the zero-point level of S_1. In addition, the relaxed vibrational levels are also observed by nonresonant two-photon ionization, which was called a NID method by Fujii's group.[19] The REMPI spectrum from the IR-pumped level shows sharp bands, whereas the NID signal from the relaxed levels exhibits broad structureless spectra across a wide energy region. We observed the decay of the OH/OD level by probing the sharp band and the rise of the relaxed levels by monitoring the broad band.

Jet-cooled phenol was generated by the supersonic expansion of a gaseous sample seeded in He carrier gas into vacuum through a pulsed nozzle (General Valve) having a 400-μm orifice. The phenol−Ar cluster was generated by using a mixed carrier gas of Ar/He with the ratio of 1:3 at a total pressure of 3 atm. The phenol−H_2O hydrogen-bonded cluster was generated by using a mixed carrier gas of H_2O/He. The jet-cooled molecules were skimmed by a skimmer (1 mm diameter) located 30 mm downstream of the nozzle. The IR and UV beams were introduced into the vacuum chamber coaxially in a counter-propagated manner and crossed the supersonic beam 50 mm downstream of the skimmer. The molecules were ionized by 1 + 1 REMPI via S_1, and the ions were repelled perpendicularly to the plane of the molecular beam and the laser beams. The

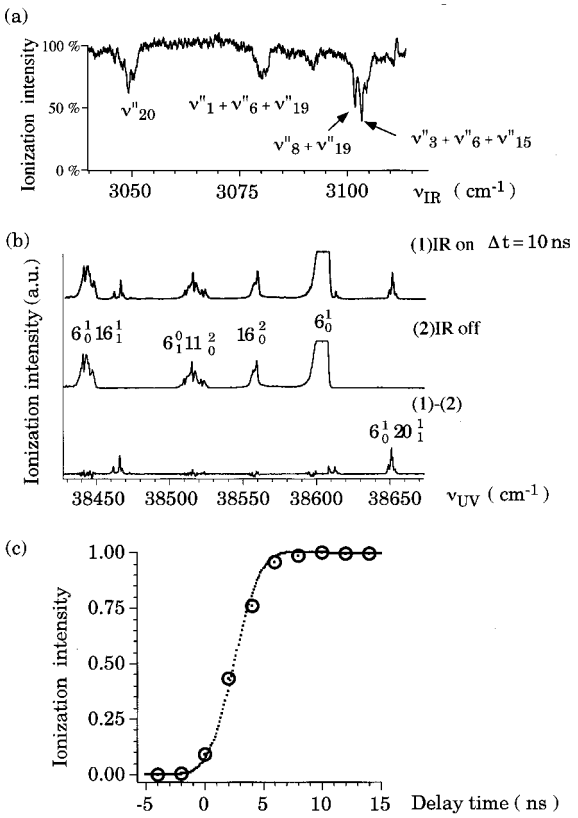

Figure 2. (a) Ionization-detected IR spectrum of the CH stretching vibration of benzene in a supersonic beam. (b) (1) IR−UV double-resonance spectrum of benzene observed at a delay time of 10 ns after the IR excitation to ν_{20}. (2) REMPI spectrum of benzene measured without the IR excitation. (3) IR−UV enhanced spectrum obtained by subtracting spectrum 2 from spectrum 1. (c) Plots of the $6_0^1 20_1^1$ band intensity vs the delay time between IR and UV lasers, where the IR and UV lasers are fixed to ν_{20}'' and the $6_0^1 20_1^1$ band, respectively. The dotted curve is the convoluted curve obtained by assuming 3 ns (fwhm) Gaussian pulses for the pump (IR) and probe (UV) pulses.

ions were mass analyzed by a 70-cm time-of-flight tube and were detected by an electron multiplier (Murata Ceratron). The ion signals were integrated by a boxcar integrator (Par model 4420/4400) and processed by a microcomputer.

The IR light (ν_{IR}) was generated by different frequency generation between the second harmonic of an injection-seeded Nd:YAG laser (Continuum PL 8000) and the output of a dye laser (Continuum ND 6000) pumped by the Nd:YAG laser with a $LiNbO_3$ crystal. The UV laser light (ν_{UV}) used for S_1-S_0 transition was the second harmonic of a dye laser (Lumonics HD 500) pumped by another Nd:YAG laser (Continuum Surelite). The resolutions of ν_{IR} and ν_{UV} were estimated to be 0.1 and 0.2 cm^{-1}, respectively. Typical output of ν_{IR} was 200 μJ, whereas that of ν_{UV} was 300 μJ. The time delay between the IR and UV pulses was controlled by a digital delay generator (SRS DG-535).

The pulse shapes of the pump and probe light pulses used were obtained by deconvolution of the IR−UV pump−probe signal for the CH stretching vibration (ν_{20}) of benzene. The 1 + 1 REMPI spectrum of the CH stretching vibration of benzene was first reported by Lee's group,[20] and we carried out the same experiment, as shown in Figure 2. Figure 2a shows the ionization-detected IR spectrum of benzene in the CH stretching vibrational region. In this experiment, ν_{UV} was fixed to the 6_0^1 band of benzene, and the ion intensity generated by 1 + 1 REMPI was monitored. Under these conditions, the ν_{IR} pulse was introduced 50 ns prior to the ν_{UV} pulse, and its frequency

TABLE 1: Values of Electronic Transition Frequencies and OH(OD) Stretching Vibrational Energies of Phenol-d_0 (Phenol-d_1) and Its Clusters[a]

	0_0^0 band	$\upsilon_{OH(OD)}\,{}_1^0$ band	$\nu_{OH(OD)}$
phenol	36 349	32 692	3657
phenol-d_1	36 347	33 647	2700
phenol−Ar	36 315	32 659	3656
phenol−H_2O	36 000	32 476	3524

[a] Values are in units of wavenumbers.

was scanned. The IR spectrum was obtained as an ion-dip spectrum. In Figure 2a, four bands are observed, and the lowest-frequency band at 3049 cm^{-1} is assigned to ν_{20}.[20] Figure 2b shows the 1 + 1 REMPI spectrum observed with and without the IR pumping to the 20_1 level. We then fixed ν_{UV} to the $20_1^1 6_0^1$ band at 38 650 cm^{-1} and measured the ion signal by changing the delay time of ν_{UV} with respect to ν_{IR}. Figure 2c shows the intensity of the $20_1^1 6_0^1$ signal vs the delay time and also the convoluted curve fit by assuming that both IR and UV pulses have a Gaussian shape with a fwhm of 3 ns. The rise of the ion signal was well-fit by the convolution, and these pulse shapes were used for other experiments. As seen in Figure 2c, the CH stretch level does not decay on this time scale. Actually, the ion intensity was almost constant even at a delay time of 100 ns, indicating very slow intramolecular vibrational redistribution (IVR) of the ν_{CH} vibration of benzene.

Phenol was purchased from Wako chemical and was purified by vacuum sublimation before use. Deuterated phenol (phenol-d_1) was synthesized by adding a few drops of D_2O to phenol in a sample housing.

Results

The frequencies of the OH stretching vibrations of bare phenol and phenol−H_2O were previously reported to be 3657 and 3524 cm^{-1}, respectively.[8,10,18] In the present work, we also observed the OH stretch band of phenol−Ar and determined its frequency to be 3656 cm^{-1}. Because Ar is bound on the phenyl plane by a vdW force, cluster formation does not significantly affect the force constant of the in-plane OH stretching mode of phenol. We also measured the OD stretching vibration of phenol-d_1 and determined its frequency to be 2700 cm^{-1}, which is in good agreement with the value reported by Bist et al.[21] The electronic transition frequencies and the energies of the OH (OD) stretching vibration of the present system are listed in Table 1. The relaxation of the OH levels was investigated by measuring the electronic spectra from the pumped level, as well as the relaxed levels, at different delay times between the IR and the UV pulses.

1. Phenol-d_0 and Phenol-d_1. Figure 3 shows the 1 + 1 REMPI spectra of the S_1−S_0 transition of bare phenol-d_0 measured at three different delay times after IR pumping to the OH stretching level. The spectra consist of sharp vibronic bands and a structureless broad background appearing across the whole region. The sharp band at 32692 cm^{-1} is assigned to the $\upsilon_{OH}\,{}_1^0$ band, and other sharp bands are also assigned to the vibronic bands from the $\upsilon''_{OH} = 1$ level. The presence of the background was first reported by Fujii and co-workers who ascribed to the nonresonant (NR) two-photon ionization.[19] As shown in Figure 3, the intensity ratio of the NR ionization signal to the sharp $\upsilon_{OH}\,{}_1^0$ band increases with the delay time.

Figure 4a shows the observed time evolution of the sharp $\upsilon_{OH}\,{}_1^0$ band and the NR ionization signal intensities, and Figure 4b shows the same time evolution normalized at each maximum. There are two noticeable points in the time evolution. First, the $\upsilon_{OH}\,{}_1^0$ band decays with two components: a fast component with a time constant of a few nanoseconds and a slow component whose intensity is almost constant within the observed time region. Second, the rate of appearance of the NR band coincides with the rate of the fast decay component of the $\upsilon_{OH}\,{}_1^0$ band. Figure 4c shows the time profile of the $\upsilon_{OH}\,{}_1^0$ band on a longer time scale, demonstrating that the slow component does not decay even at 200 ns after the IR excitation. The coincidence of the decay time of the fast component and the appearance time of the NR background signal indicates that the NR signal is due to the transition originating from the relaxed levels, which are populated after IVR from the optically pumped OH stretch level.

We then measured the IR spectra of the OH stretch vibration by fixing the UV laser frequency to the sharp $\upsilon_{OH}\,{}_1^0$ band and the broad band, which are shown in Figure 5b and c. As seen in the figure, although both vibrational spectra show similar OH stretching bands of phenol, there is a slight difference in their rotational envelopes. This difference is attributed to the difference of the rotational levels probed by ν_{UV} in the two measurements. The bandwidth of ν_{UV} (0.2 cm^{-1}) is narrower than that of the rotational envelope of the electronic band, as shown in Figure 5a. This means that only a limited number of the rotational levels of $\upsilon''_{OH} = 1$ are probed when the UV laser is fixed to the $\upsilon_{OH}\,{}_1^0$ band. On the other hand, no rotational-level selection is involved in NR ionization detection as the intermediate state in the ionization process is the virtual state, and all of the rotational levels of $\upsilon''_{OH} = 1$, pumped by ν_{IR}, are probed. This is the reason why the IR spectrum obtained by monitoring the NR ionization is wider than that obtained by monitoring the $\upsilon_{OH}\,{}_1^0$ band detection.

Similar experiments have been performed for the OD stretching vibration of phenol-d_1. Figure 6a shows the MPI spectra of bare phenol-d_1 measured at three different delay times after the IR excitation to its OD stretch level at 2700 cm^{-1}. Although the spectra also consist of sharp vibronic bands and the NR background, the ratio of the NR signal to the sharp vibronic bands of phenol-d_1 is much smaller than that of phenol-d_0. Figure 6b shows the time profile of the sharp $\upsilon_{OD}\,{}_1^0$ band and the NR signal. Unlike phenol-d_0, a fast decay component is not seen for the $\upsilon_{OD}\,{}_1^0$ band, and its signal intensity is constant within the observed time region. On the other hand, the broad background signal appears a few nanoseconds later with respect to the sharp $\upsilon_{OH}\,{}_1^0$ band, which is similar to phenol-d_0.

The observed electronic spectra and the time evolution of the OH and OD stretching vibrations of phenol will be interpreted in terms of the intermediate-coupling scheme of the IVR process. We return to the coupling scheme of IVR shown in Figure 1b. In the zeroth-order description, the IR light pulse initially prepares the state $|\upsilon_{OH(OD)} = 1, \upsilon_l = 0\rangle$, where the υ_l represent vibrational quantum number(s) of the sparse manifold $\{l\}$. The sparse manifold $\{l\}$ consists of a set of vibrational levels that are coupled with $\upsilon_{OH(OD)} = 1$ through the anharmonic coupling $\mathbf{W}_{strong}$. Then, IVR takes place from the initially prepared state to the states $|\upsilon_{OH(OD)} = 0, \upsilon_l = \upsilon\rangle$. The interaction energy, Γ, is expressed by

$$\Gamma = 2\pi|\mathbf{W}_{strong}|^2\rho_l$$

where ρ_l is the vibrational density of states in the $\{l\}$ manifold. The sparse manifold may be further coupled to the bath mode $\{b\}$ with an interaction energy of γ, which is proportional to the square of $\mathbf{W}_{weak}$. The total vibrational density of states, ρ_l, is estimated by a direct counting method using the vibrational

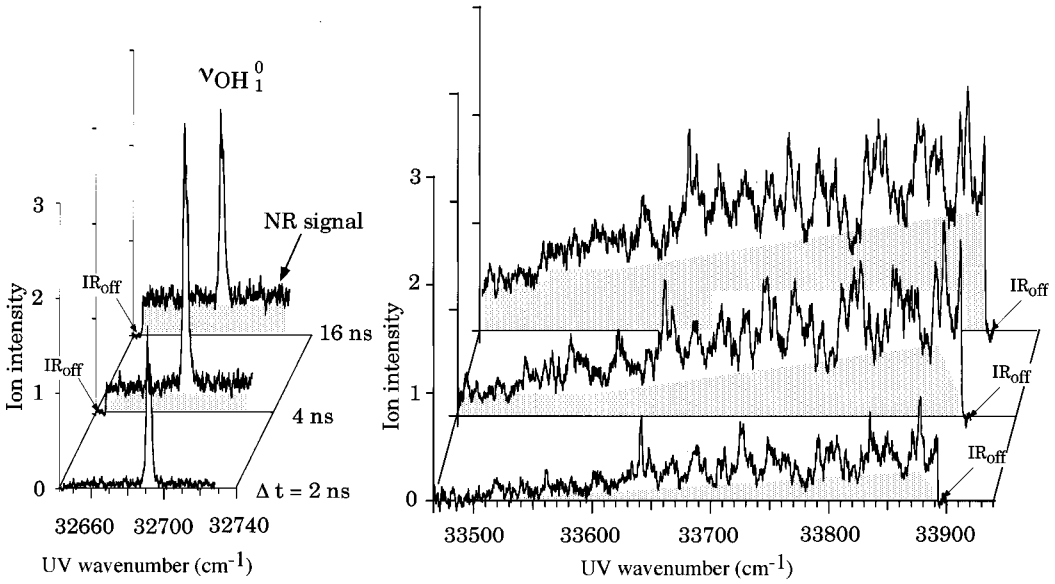

Figure 3. IR−UV double-resonance spectra of phenol observed at three different delay times after the IR excitation to the OH stretch vibration. Hatched parts in the spectra are the nonresonant (NR) two-photon ionization from the levels generated by IVR.

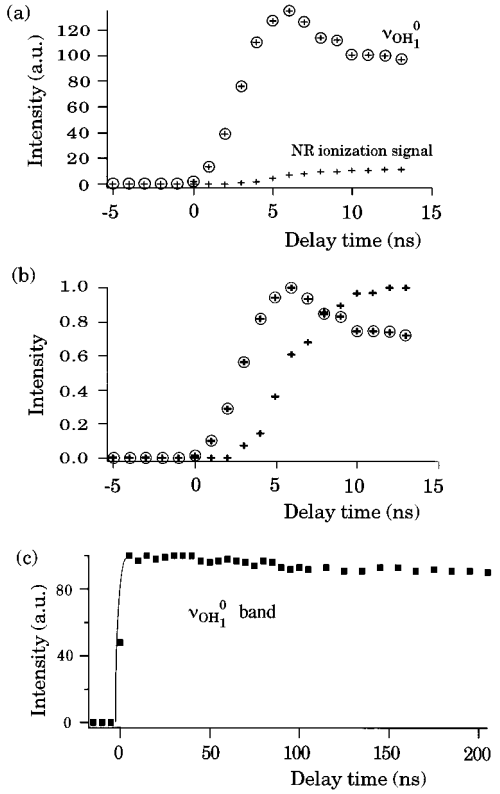

Figure 4. (a) Plots of the sharp $\upsilon_{OH}{}_1^0$ and NR background signal intensities vs the delay time. In the latter, the UV frequency was fixed to 32 800 cm^{-1}. (b) Time evolution of the $\upsilon_{OH}{}_1^0$ and broad bands whose intensities are normalized to their maximum intensities. (c) Intensity of $\upsilon_{OH}{}_1^0$ band vs the delay time up to 200 ns. The signals were observed every 5 ns.

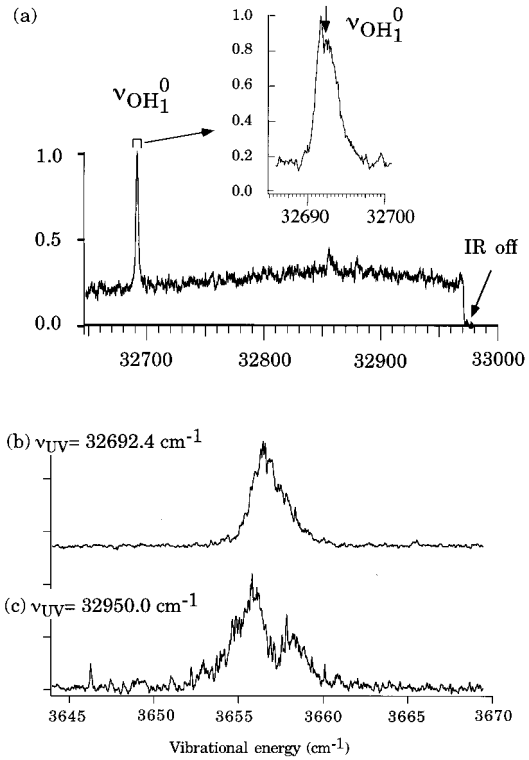

Figure 5. (a) IR−UV double-resonance spectrum of phenol. The inset is the enlarged portion of the $\upsilon_{OH}{}_1^0$ band. (b) IR spectra of the OH stretching vibrational of phenol obtained by monitoring the $\upsilon_{OH}{}_1^0$ band. (c) IR spectra obtained by fixing the UV laser to the NR background at 32950 cm^{-1}.

frequencies reported by Bist et al.,[21] yielding 500 and 50 cm^{-1} for the OH stretch of phenol-d_0 and OD stretch of phenol-d_1, respectively. Among them, only limited vibrational levels belongs to the sparse manifold $\{l\}$. Although there is not a clear criterion for defining the sparse manifold $\{l\}$, we can exclude higher-order anharmonic coupling for the strong interaction between $|\upsilon_{OH(OD)} = 1, \upsilon_l = 0\rangle$ and $|\upsilon_{OH(OD)} = 0, \upsilon_l = \upsilon\rangle$. In this respect, we assume that the manifold $\{l\}$ consists of the vibrational levels that satisfy the relation $\Delta\upsilon = \upsilon - 1 \leq 5$. Then, the density of states that couple with the OH and OD stretch is reduced to 14 and 5 cm^{-1}, respectively. Thus, the scheme can be assigned to the intermediate-strong-coupling regime.

The pulsed nanosecond laser system used in the present work does not generate a Fourier transform-limited pulse, so it may prepare the molecules incoherently in the vibrationally excited level and a quantum beat may not be observed. In this case, the initially prepared state $|\upsilon_{OH(OD)} = 1, \upsilon_l = 0\rangle$ decays with

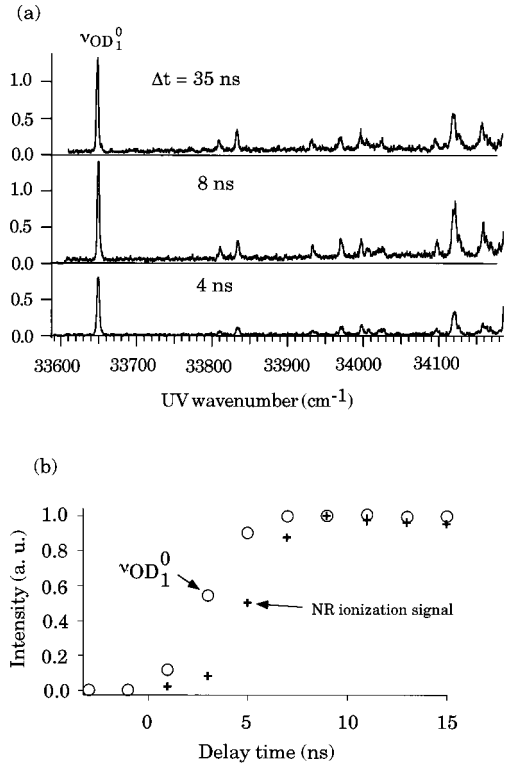

Figure 6. (a) IR−UV double-resonance spectra of phenol-d_1 observed at three different delay times after IR excitation to the OD stretching vibration. (b) Plots of the sharp $\upsilon_{OH}{}^0_1$ band and the NR signal (UV laser frequency is fixed to 33 700 cm^{-1}) intensities vs the delay time. The signal intensities are normalized to the maximum intensity of each curve.

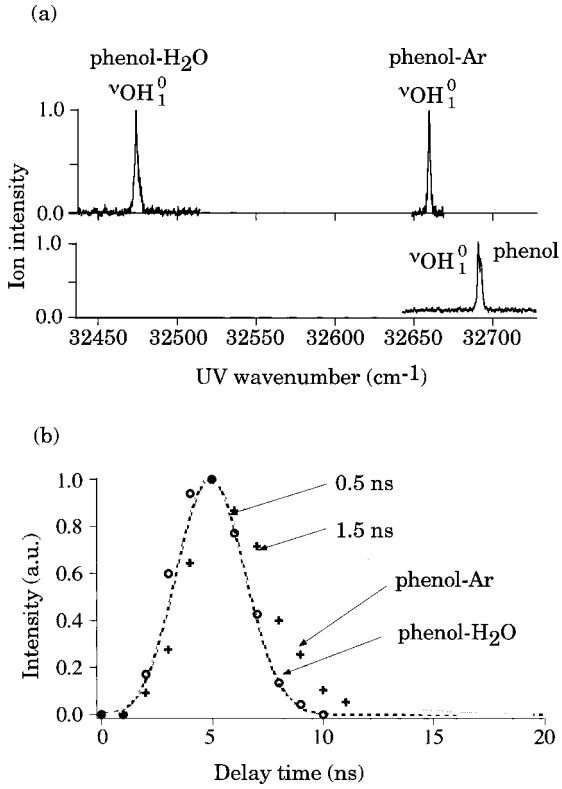

Figure 7. (a) IR−UV double-resonance spectra of the $\upsilon_{OH}{}^0_1$ band region of phenol and its clusters with Ar and H_2O observed at a delay time of 4 ns after IR excitation of the OH stretching vibrations. (b) Plots of the $\upsilon_{OH}{}^0_1$ band intensities of phenol−Ar and −H_2O vs the delay time. Convoluted curves are also shown in the figure. See text.

two components,[22] with its fast component determined by Γ and a slow component depending on the width of each level of $\{l\}$. As seen in phenol-d_0, the above characteristics of the temporal behavior agree with the observed results. Although the fast decay rate should correspond to the coupling width Γ between the OH stretch and $\{l\}$, we could not experimentally obtain its precise value because the fast component is very close to or shorter than the pulse width of the laser used.

For phenol-d_1, the intensity of the broad background transition due to the relaxed levels is much weaker than that of phenol, as seen in Figure 6a. In addition, the decay profile of the $\upsilon_{OD}{}^0_1$ band does not show two components. The differences in the spectral and temporal characteristics between phenol-d_0 and phenol-d_1 can be explained by a smaller number of vibrational levels of $\{l\}_{(OD)}$ for the OD stretch of phenol-d_1 than for the OH stretch of phenol. In the intermediate-strong coupling, the ratio of the fast to the slow components is given by $N + 1$, where N is the number of the vibrational levels in the sparse manifold.[22,23] As described above, the number of levels in the sparse manifold for the OD stretch of phenol-d_1 is smaller than that for the OH stretch of phenol. Thus, the ratio of the fast to the slow component is larger for phenol-d_0 than for phenol-d_1, and also the electronic transition from the bath mode is stronger in the former than the latter. It should be noted that the rise time of the bath mode of phenol-d_1 is not very different from that of phenol-d_0. The result indicates that the interaction energy between the OD stretch and $\{l\}_{(OD)}$ is not very different from that between the OH stretch and $\{l\}_{(OH)}$.

2. Phenol−Ar and Phenol−H_2O. Figure 7a shows the 1 + 1 REMPI spectra of in the $\upsilon_{OH}{}^0_1$ band region of phenol, phenol−Ar, and phenol−H_2O measured at a delay time of 4 ns after the IR excitation of their OH stretch vibrations. In the electronic spectra of phenol−Ar and phenol−H_2O, only the sharp $\upsilon_{OH}{}^0_1$ bands appear, and no NR background signal is observed, unlike the case for phenol. Figure 7b shows the decay of their $\upsilon_{OH}{}^0_1$ bands. As seen in the figure, both bands show very rapid decay without any slow components. Each decay curve was convoluted with a single-exponential decay constant by assuming that the IR and UV pulses have a Gaussian shape of 3 ns fwhm. The lifetimes obtained in this way are 1.5 ns for phenol−Ar and 0.5 ns for phenol−H_2O. Because their lifetimes are shorter than the laser pulse width, the obtained values may have a large uncertainty.

In phenol−Ar, Ar is known to be bound on the phenyl plane by vdW interactions. The coupling between the vdW modes and the OH vibration is very weak in phenol, so that the magnitudes of Δ and γ are expected to be not very different from those of bare phenol. However, the presence of low-frequency vdW modes drastically increases the vibrational density of states of the bath mode $\{b\}$. We also estimated the density of states of phenol−Ar by using the reported vdW vibrational frequencies.[24] The estimated density of states of phenol−Ar at 3656 cm^{-1} is $\sim 5 \times 10^6$ cm^{-1}, which is 10^4 times larger than that of bare phenol. Furthermore, the energy of the OH stretching vibration is much larger than the vdW binding energy of phenol and Ar, so that the bath mode $\{b\}$ includes the dissociation continuum. Thus, the decay of phenol−Ar is described by the statistical-limit case, resulting in a single-exponential decay.

In phenol−H_2O, the calculated vibrational density of states is similar to that of phenol−Ar. On the other hand, the coupling between the phenolic OH and the intermolecular mode is expected to be much stronger, as a frequency reduction as large as 133 cm^{-1} is observed for the OH stretching vibration upon

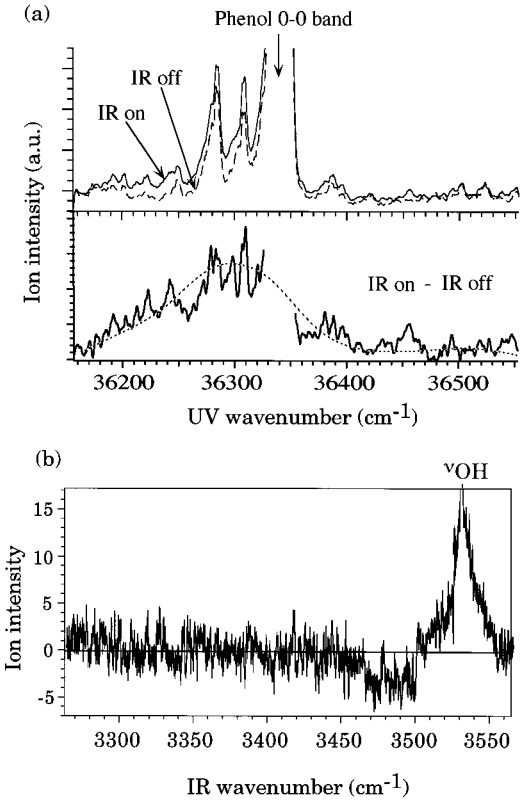

Figure 8. 1 + 1 REMPI spectra of phenol in the 0,0 band region with and without the IR excitation to the OH stretching vibration. (b) IR action spectrum obtained by fixing the UV laser frequency at 36 290 cm^{-1}.

hydrogen-bond formation. Thus, the observed larger IVR decay rate of phenol$-H_2O$ is attributed to the larger $\mathbf{W}_{strong}$ for phenol$-H_2O$ than for phenol$-$Ar.

The binding energy of phenol$-H_2O$ was determined to be 1960 cm^{-1} (242 meV) by Courty et al.[25] This value is close to the binding energy of 1-naphthol$-H_2O$ (2040 cm^{-1}) reported by Bürgi et al.[26] Thus, the energy of the OH stretching vibration is substantially larger than the dissociation energy of the hydrogen bond. Consequently, we tried to observe the dissociation fragment after IR excitation to the OH stretching vibration of phenol$-H_2O$. Figure 8a shows the 1 + 1 REMPI spectrum of the 0,0 band region after at the delay time of 30 ns after the IR excitation of the hydrogen-bonded OH stretch of phenolic site. As seen in the figure, a broad hot band due to the phenol fragment is observed in the lower-frequency region of the 0,0 band of phenol. Figure 8b shows the IR action spectrum obtained by monitoring the broad band at 36 290 cm^{-1}. The band at 3530 cm^{-1} in the action spectrum is assigned to the hydrogen-bonded OH stretching vibration of phenol. The result clearly shows that the bare phenol is generated as a fragment from phenol$-H_2O$ after the IR excitation of its OH stretching vibration. It may be very interesting to investigate whether the dissociation occurs after complete energy randomization within the cluster or places through direct coupling between the OH stretch and the intermolecular mode. Although we tried to observe the rise of the fragment signal, the signal-to-noise ratio was not good enough to discuss the time profile, and it remains a problem to be solved in near future.

Conclusion

Nanosecond IR$-$UV pump probe double-resonant spectroscopy has been applied to the relaxation the OH stretching vibration of jet-cooled phenol and its clusters. The investigation has been performed by observing the time evolution of the pumped level as well as the relaxed levels. It was found that the IVR of the OH stretch vibration of bare phenol is assigned to the intermediate-coupling scheme. On the other hand, the OH stretch levels of phenol$-$Ar and $-H_2O$ showed a switch from the intermediate case to the statistical limit through cluster formation. It was also found that the IVR rate of phenol$-H_2O$ is larger than that of phenol$-$Ar, which is explained by the stronger anharmonic coupling between OH and intermolecular mode in the former cluster than in the latter.

References and Notes

(1) For example, see: Pimentel, G. C.; McClellan, A. L. *The hydrogen bond*; W. H. Freeman and Company: San Francisco, 1960.
(2) Laubereau, A.; Kaiser, W. *Rev. Mod. Phys.* **1978**, *50*, 607.
(3) Oxtoby, D. W. *Annu. Rev. Phys. Chem.* **1981**, *32*, 77.
(4) Kaiser, W. *Ultrashort laser pulses and applications*; Springer: Berlin, 1988.
(5) Heilweil, E. J.; Casassa, M. P.; Cavanagh, R. R.; Stephenson, J. C. *Annu. Rev. Phys. Chem.* **1989**, *40*, 143.
(6) Elsaesser T.; Kaiser, W. *Annu. Rev. Phys. Chem.* **1991**, *42*, 83.
(7) Owrutsky, J. C.; Raftery, D.; Hochstrasser, R. M. *Annu. Rev. Phys. Chem.* **1994**, *45*, 519.
(8) Tanabe, S.; Ebata, T.; Fujii, M.; Mikami, N. *Chem. Phys. Lett.* **1993**, *215*, 347.
(9) Ebata, T.; Watanabe, T.; Mikami, N. *J. Phys. Chem.* **1995**, *99*, 5761.
(10) Watanabe, T.; Ebata, T.; Tanabe, S.; Mikami, N. *J. Chem. Phys.* **1996**, *105*, 408.
(11) Iwasaki, A.; Fujii, A.; Watanabe, T.; Ebata T.; Mikami, N. *J. Phys. Chem.* **1996**, *100*, 16053.
(12) Matsumoto, Y.; Ebata, T.; Mikami, N. *J. Chem. Phys.* **1998**, *109*, 6303.
(13) Matsumoto, Y.; Ebata, T.; Mikami, N. *J. Mol. Struct.*, in press.
(14) Mitsuzuka, A.; Fujii, A.; Ebata, T.; Mikami, N. *J. Chem. Phys.* **1996**, *105*, 2618.
(15) Mitsuzuka, A.; Fujii, A.; Ebata, T.; Mikami, N. *J. Phys. Chem. A* **1998**, *102*, 9779.
(16) Guchhait, N.; Ebata, T.; Mikami, N. *J. Am. Chem. Soc.* **1999**, *121*, 5705.
(17) Guchhait, N.; Ebata, T.; Mikami, N. *J. Chem. Phys.* **1999**, *111*, 8438.
(18) Hartland, G. V.; Henson, B. F.; Venturo, V. A.; Felker, P. M. *J. Phys. Chem.* **1992**, *96*, 1164.
(19) Ishiuchi, S.; Shitomi, H.; Takazawa, K.; Fujii, M. *Chem. Phys. Lett.* **1998**, *283*, 243.
(20) Page, R. H.; Shen, Y. R.; Lee, Y. T. *J. Chem. Phys.* **1988**, *88*, 5362.
(21) Bist, H. D.; Brand, J. C. D.; Williams, D. R. *J. Mol. Spectrosc.* **1967**, *24*, 402.
(22) Freed, K. F.; Nitzan, A. *J. Chem. Phys.* **1980**, *73*, 4765.
(23) Lahmani, F.; Tramer, A.; Tric, C. *J. Chem. Phys.* **1974**, *60*, 4431.
(24) Mons, M.; Le Calvé, J.; Piuzzi, F.; Dimicoli, I. *J. Chem. Phys.* **1990**, *92*, 2155.
(25) Courty, A.; Mons, M.; Dimicoli, I.; Piuzzi, F.; Brenner V.; Millié, P. *J. Phys. Chem.* **1998**, *102*, 4890.
(26) Bürgi, T.; Droz, T.; Leutwyler, S. *Chem. Phys. Lett.* **1995**, *246*, 291.